The membrane scaffold CD82 regulates cell adhesion by altering α4 integrin stability and molecular density

Christina M. Termini[a], Maura L. Cotter[a], Kristopher D. Marjon[a], Tione Buranda[a], Keith A. Lidke[b], and Jennifer M. Gillette[a]

[a]Department of Pathology, University of New Mexico Health Sciences Center, and [b]Department of Physics and Astronomy, University of New Mexico, Albuquerque, NM 87131

ABSTRACT **Hematopoietic stem/progenitor cell (HSPC) interactions with the bone marrow microenvironment are important for maintaining HSPC self-renewal and differentiation. In recent work, we identified the tetraspanin protein, CD82, as a regulator of HPSC adhesion and homing to the bone marrow, although the mechanism by which CD82 mediated adhesion was unclear. In the present study, we determine that CD82 expression alters cell–matrix adhesion, as well as integrin surface expression. By combining the superresolution microscopy imaging technique, direct stochastic optical reconstruction microscopy, with protein clustering algorithms, we identify a critical role for CD82 in regulating the membrane organization of α4 integrin subunits. Our data demonstrate that CD82 overexpression increases the molecular density of α4 within membrane clusters, thereby increasing cellular adhesion. Furthermore, we find that the tight packing of α4 into membrane clusters depend on CD82 palmitoylation and the presence of α4 integrin ligands. In combination, these results provide unique quantifiable evidence of CD82's contribution to the spatial arrangement of integrins within the plasma membrane and suggest that regulation of integrin density by tetraspanins is a critical component of cell adhesion.**

Monitoring Editor
Mark H. Ginsberg
University of California, San Diego

Received: Nov 13, 2013
Revised: Mar 3, 2014
Accepted: Mar 5, 2014

INTRODUCTION

Cells receive signals or cues from their surrounding environment and respond so as to optimize survival, maintain quiescence, and promote proliferation, and differentiation. Stem cells, in particular, rely on physical interactions with their surrounding microenvironment or "niche" for the regulation and maintenance of their proper function. In the case of hematopoietic stem/progenitor cells (HSPCs), which reside primarily in the bone marrow, direct contact with the surrounding microenvironment is essential for regulating their proliferation, multipotentiation, and self-renewal (Zhang and Li, 2008; ter Huurne *et al.*, 2010). The bone marrow niche is a complex microenvironment consisting of a number of different cellular and extracellular matrix (ECM) components, including fibronectin and collagen I, III, and IV, as well as laminin (Klein, 1995). In addition to the bone marrow, HSPCs can traffic into and out of the peripheral blood, which is used clinically for stem cell isolation and transplantation. Furthermore, under stress conditions and/or injury, HSPCs can migrate to other tissues, such as spleen, liver, and even heart, to aid in tissue repair and remodeling (Taniguchi *et al.*, 1996; Oostendorp *et al.*, 2000; Losordo *et al.*, 2011). However, molecular mechanisms orchestrating the interactions between HSPCs and various niche components are not well understood.

The tetraspanins are a family of multispanning membrane scaffold proteins that regulate intercellular interactions. CD82 (also known as Kai1) is a member of the tetraspanin family of proteins, which are evolutionarily conserved proteins present in most eukaryotes and function in many aspects of cell physiology as mediators of cell adhesion, membrane trafficking, and cell signaling (Charrin

This article was published online ahead of print in MBoC in Press (http://www.molbiolcell.org/cgi/doi/10.1091/mbc.E13-11-0660) on March 12, 2014.

Address correspondence to: Jennifer M. Gillette (jgillette@salud.unm.edu).

Abbreviations used: CD82KD, KG1a-knockdown cells created with CD82 short hairpin RNAs; CD82OE, KG1a cells that overexpress CD82 tagged with the mCherry fluorescent protein; dSTORM, direct stochastic optical reconstruction microscopy; ECM, extracellular matrix; HSPC, hematopoietic stem and progenitor cell; LDV, leucine–aspartic acid–valine sequence; Palm-CD82OE, KG1a cells that overexpress a palmitoylation-deficient form of CD82 tagged with the mCherry fluorescent protein; TEM, tetraspanin-enriched microdomain.

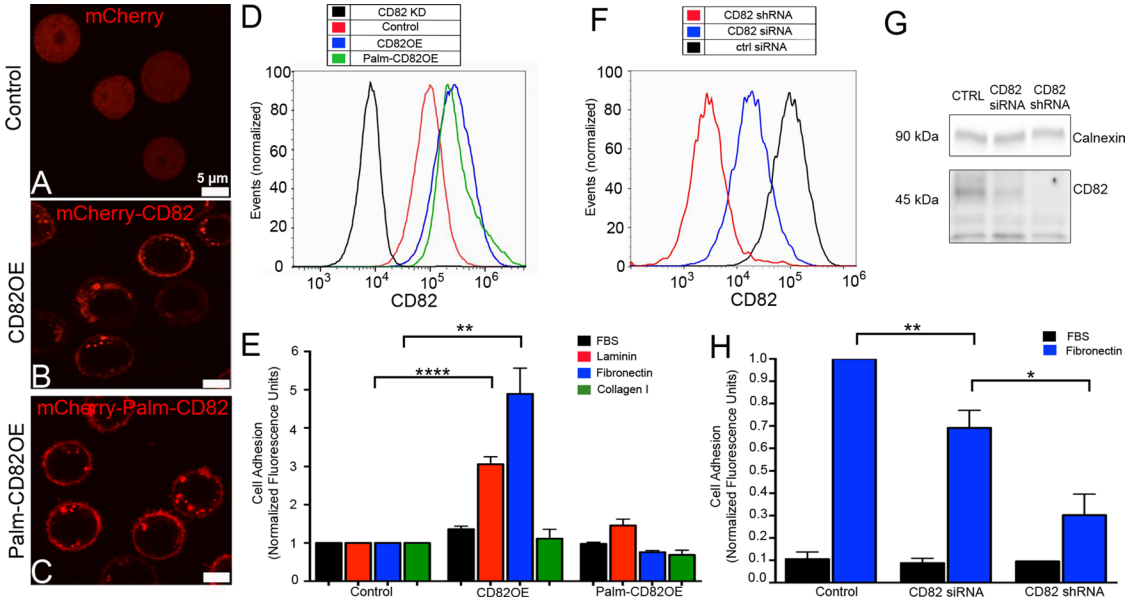

FIGURE 1: CD82 expression mediates HSPC adhesion to fibronectin. Epifluorescence images depicting stable KG1a cell lines generated with (A) mCherry, (B) mCherry-CD82, and (C) mCherry-Palm-CD82 constructs. (D) The surface expression of CD82 was analyzed for each cell line using flow cytometry. (E) Cellular adhesion of each cell line was measured using a fluorescence-based adhesion assay. Cells were plated on FBS as a control or the indicated ECM proteins. To knock down CD82, KG1a cells were transfected with control siRNA, CD82 siRNA, and CD82 shRNA. The reduction of CD82 surface and total expression was measured by flow cytometry (F) and Western blot analysis (G). The adhesive abilities of these KD cells were then measured with the fluorescence adhesion assay (H). Error bars, SD; $n \geq 3$ (*$p < 0.05$, **$p < 0.01$, ****$p < 0.0001$).

et al., 2009). One of the most distinct features of tetraspanins is their ability to associate in *cis* with other tetraspanins, integrins, members of the immunoglobulin superfamily of cell adhesion molecules, and signaling receptors, thereby forming tetraspanin-enriched microdomains (TEMs; Hemler, 2008; Charrin *et al.*, 2009; Bassani and Cingolani, 2012). Formation of TEMs enables tetraspanins to serve as molecular facilitators or organizers for a number of transmembrane proteins. Tetraspanins also recruit and maintain intracellular signaling molecules in close proximity with membrane proteins, thus regulating downstream biochemical pathways (Hemler, 2005; Wang *et al.*, 2007; Choi *et al.*, 2009; Li *et al.*, 2010).

In its role as a protein scaffold, CD82 can form TEMs, hypothesized to be critical for the organization and function of several membrane proteins, including integrins (He *et al.*, 2005; Han *et al.*, 2012). Integrins are heterodimeric cell adhesion receptors consisting of one α- and one β-subunit and are expressed by all multicellular organisms. Components of the ECM, as well as specific cell surface receptors, serve as integrin ligands (Harburger and Calderwood, 2009; Barczyk *et al.*, 2010). Integrins are capable of transmitting signals across the plasma membrane, which can promote cell migration, survival, differentiation and motility. Specifically, the α4 integrin, which is highly enriched in HSPCs, regulates HSPC migration, homing, proliferation, and differentiation (Coulombel *et al.*, 1997; Arroyo *et al.*, 1999). Furthermore, previous studies in mice show that defects occur in HSPC homing and short-term engraftment upon conditional α4 knockout (Scott *et al.*, 2003), and anti-α4β1antibodies mobilize HSPCs into the bloodstream (Papayannopoulou and Nakamoto, 1993). How CD82 can regulate integrin-mediated cellular and molecular functions including migration, adhesion, and signaling remains unclear. Furthermore, fundamental questions concerning the formation and regulation of TEMs and their potential modulation of integrin organization also still exist.

Previous work from our lab identified CD82 as a regulator of HSPC homing and osteoblast adhesion (Larochelle *et al.*, 2012). Using monoclonal antibodies specific to CD82, we demonstrated an inhibition of HSPC homing to the bone marrow and were able to reduce HSPC adhesion to osteoblasts. In the present study, we set out to identify the mechanism by which CD82 regulates HSPC niche interactions. We find that CD82 expression alters integrin expression by contributing to integrin stabilization on the plasma membrane via modulation of integrin internalization and recycling. Furthermore, we apply direct stochastic optical reconstruction microscopy (dSTORM) analysis to evaluate how CD82 and modifications in the palmitoylation sites of CD82 regulate the nanoscale clustering of integrins. Our data suggest that CD82 modulates the molecular packing of α4 molecules within clusters, thereby regulating the local molecular density of α4. As such, CD82 functionally regulates niche adhesion by modifying the organization of integrins into tightly packed clusters, which serves to strengthen cell adhesion to the ECM.

RESULTS

CD82 expression regulates cell–matrix adhesion

To begin analyzing the molecular mechanism by which CD82 regulates HSPC interactions with niche components, we generated a CD82-overexpressing cell line using human acute myelogenous leukemia progenitor-like cells, KG1a. We created a fusion protein in which CD82 was tagged with the mCherry fluorescent protein at the amino terminus (CD82OE). Stably transfected cells were selected and sorted. Figure 1B illustrates the plasma membrane and endosomal localization of mCherry-CD82, which is consistent with the localization of endogenously expressed CD82 (Larochelle *et al.*, 2012). A stably expressing mCherry control cell line (control) was also generated (Figure 1A). Flow cytometry analysis indicates a

twofold increase in CD82 surface expression between overexpressing and control cells (Figure 1D). Because our previous data suggested that CD82-specific antibodies alter in vitro adhesion and in vivo homing, we evaluated the CD82OE cells for changes in ECM adhesion. Using a fluorescence-based adhesion assay to quantify changes in cell–matrix adhesion to various substrates, we identified an increase in cell adhesion with CD82OE cells (Figure 1E). More specifically, we found that CD82OE cells display an increase in cell adhesion to laminin and an even greater increase in adhesion to fibronectin compared with control cells. Similarly, we found that reduction of CD82 expression could also affect cell–matrix adhesion. CD82-knockdown (CD82KD) cells were generated in the KG1a cell line using small interfering RNA (siRNA) and short hairpin RNA (shRNA). The CD82KD cells were found to express <10% of wild-type CD82 expression, as determined by Western blot and flow cytometry analysis (Figure 1, F and G). When CD82KD cells were assessed for cell adhesion, we detected a significant decrease in cell–matrix adhesion to fibronectin (Figure 1H), which was rescued when CD82KD cells were transiently transfected with mCherry-CD82 (Supplemental Figure S1, A–D). In combination, these data suggest a role for CD82 expression in regulation of cell–matrix adhesion.

The function of CD82 as a molecular organizer can be regulated by the ability of CD82 to cluster and form TEMs. Based primarily on biochemical studies, palmitoylation of the intracellular cysteines of tetraspanins has been suggested to play an important role in the maintenance of tetraspanin–tetraspanin interactions and to facilitate the oligomerization and dynamic reorganization of proteins into TEMs (Berditchevski *et al.*, 2002; Charrin *et al.*, 2002; Yang *et al.*, 2002; Kovalenko *et al.*, 2004). To assess whether the five membrane-proximal cysteine residues known to be palmitoylated in CD82 are critical for HSPC adhesion, we generated KG1a cells that overexpress a palmitoylation-deficient form of CD82 tagged with the mCherry fluorescent protein (Palm-CD82OE). The Palm-CD82 construct was generated by mutating the five cysteine residues at 5, 74, 83, 251, and 253 to serine, thereby preventing their palmitoylation (Mazurov *et al.*, 2007). Characterization of the Palm-CD82OE cells indicates that the localization and expression of mCherry-Palm-CD82 is consistent with that of mCherry-CD82 based on epifluorescence imaging (Figure 1C) and flow cytometry analysis (Figure 1D). To assess whether the palmitoylation sites alter the ability of CD82 to regulate cell–matrix adhesion, we performed matrix adhesion assays with the Palm-CD82OE cells and found a significant decrease in adhesion when compared with the CD82OE cells (Figure 1E). These data indicate that the palmitoylation of CD82 is essential for its ability to regulate cell–matrix adhesion.

CD82 expression modifies the profile of surface integrin expression

Cell adhesion to ECM proteins such as laminin and fibronectin occurs through specific integrin heterodimers. Tetraspanins form complexes with integrins, which can regulate ligand-binding and integrin-signaling properties (Nishiuchi *et al.*, 2005; Sridhar and Miranti, 2006; Kotha *et al.*, 2008). Furthermore, recent studies suggest that tetraspanins can also regulate integrin trafficking and complex assembly (He *et al.*, 2005; Liu *et al.*, 2007; Xu *et al.*, 2009). Therefore we set out to determine whether CD82 expression levels affect the surface expression of specific integrins that are critical for HSPC adhesion. Flow cytometry analysis suggests that, whereas levels of CD82 expression have minimal effect on α3, α5, β1, or β7 surface levels (Figure 2D and Supplemental Figure S2), CD82 overexpression results in an increase in α2 and α4 expression (Figure 2, A and B). This observed increase in α2 and α4 is consistent with the detected increase in adhesion to laminin and fibronectin, respectively (Figure 1E). In contrast, we detect a significant reduction in α6 expression in CD82OE and Palm-CD82OE cells. This decrease in α6 likely results in the availability of β1 to bind to α4, which could explain the lack of β1 expression increase in the CD82OE cells (Figure 2C). Our cytometry data also indicate that CD82KD results in decrease of α2 and α4 surface expression (Figure 2, A and B). In combination, these data suggest that modifications in CD82 expression levels can serve to regulate the surface expression of specific integrins.

CD82-mediated adhesion to fibronectin is modulated by the α4β1 integrin

On the surface of HSPCs, the predominant integrins involved in fibronectin binding are αVβ3, α5β1, α4β7, and α4β1 (Coulombel *et al.*, 1997; Mazo *et al.*, 2011). Of these fibronectin-binding integrins, α4β1 is well established as a critical regulator of HSPC/niche cell contact, mobilization, and homing. Because CD82 was described previously to interact with α4β1 (Mannion *et al.*, 1996), we first analyzed the localization of CD82 with respect to the α4 integrin. Confocal images in Figure 2E suggest a similar membrane localization of CD82 with α4, further indicating a potential interaction. To determine more specifically whether CD82-mediated increase in fibronectin adhesion occurs through regulation of α4β1, we added a specific blocking peptide to the adhesion assay. Using a saturating concentration (1 μM) of the α4β1-specific monovalent ligand leucine–aspartic acid–valine sequence (LDV), which binds to α4β1 and subsequently blocks its function (Jackson *et al.*, 1997), we observed an inhibition of CD82-mediated increase in adhesion to fibronectin (Figure 2F). These data suggest that CD82-mediated adhesion to fibronectin involves the α4β1 integrin. In addition to fibronectin, we also evaluated adhesion to the α4β1-specific ligand vascular cell adhesion molecule-1 (VCAM-1; Supplemental Figure S3). Consistent with our fibronectin data, CD82 expression also regulates adhesion to VCAM-1, further supporting involvement of the α4β1 integrin.

Next we evaluated whether CD82 alters global expression levels of either α4 or β1, which could affect cell adhesion to fibronectin. Western blot analysis indicates that CD82 overexpression increases the expression of mature and immature forms of α4 (Figure 2G). Based on densitometry analysis, the increase in mature α4 expression is ~20%, which correlates with the increase in α4 surface expression observed by flow cytometry. Overexpression of the Palm-CD82 mutant also results in an increase in α4 expression (Figure 2G), whereas knockdown of CD82 using siRNAs or shRNAs leads to decreased expression of α4 (Figure 2H) with no perturbations of β1 expression (Figure 2J). Similarly, we were unable to detect differences in β1 expression in the CD82OE or Palm-CD82OE cells by Western blot analysis (Figure 2I). In addition, we were unable to detect direct interaction between CD82 and α4 via immunoprecipitation analysis, consistent with previous reports (Serru *et al.*, 1999; Supplemental Figure S4A). Finally, evaluation of α4 mRNA levels by real-time PCR indicates that the α4 expression decrease in CD82KD cells does not result from changes in mRNA expression (Supplemental Figure S4B). These data suggest that CD82 alters the integrin expression profile of the cells and specifically affects α4 expression, which may alter cell–fibronectin adhesion.

CD82 expression alters the endocytosis and recycling of α4 integrin

Recently a number of tetraspanins, including CD82, were shown to regulate integrin turnover during *Drosophila* oocyte development

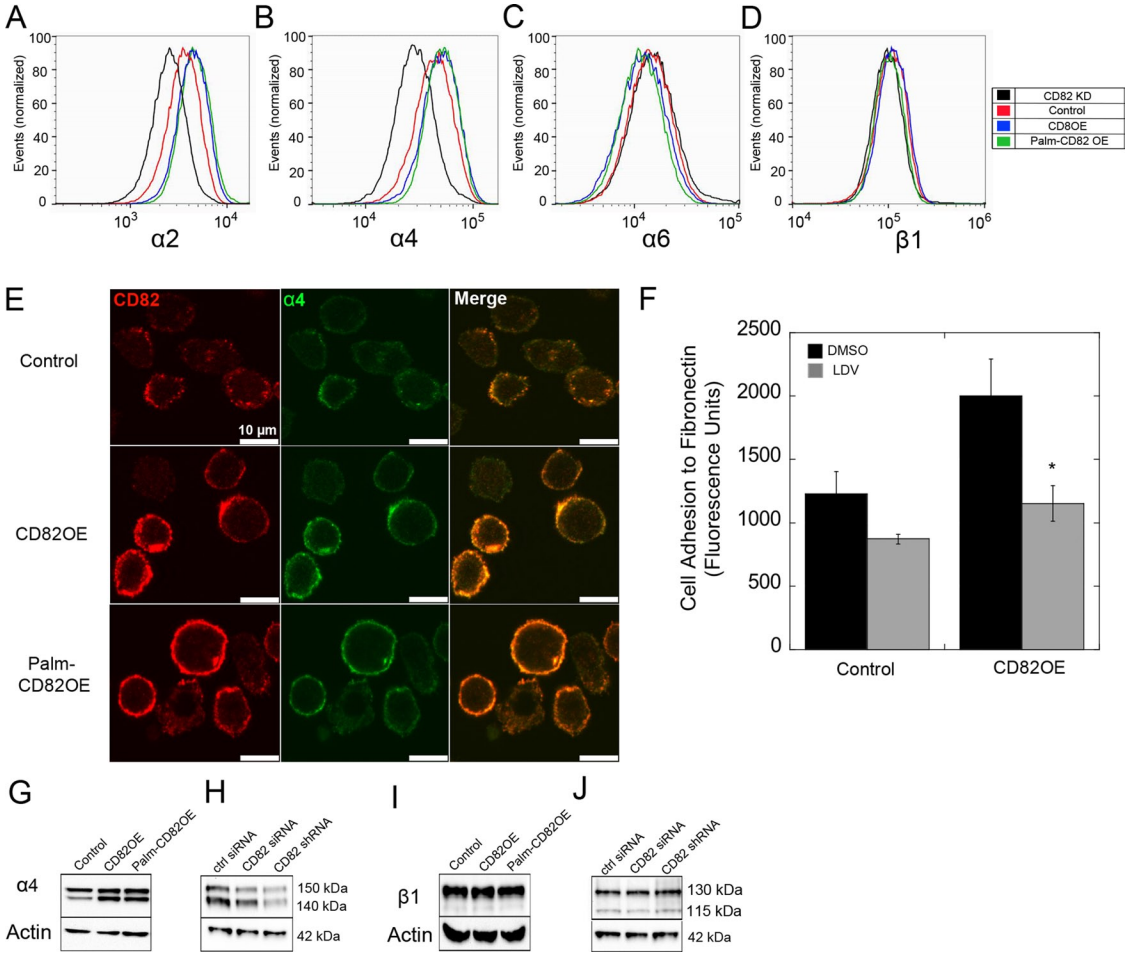

FIGURE 2: CD82 expression modulates integrin expression. Protein surface expression was assessed by flow cytometry for the (A) α2, (B) α4, (C) α6, and (D) β1 integrin subunits. (E) Confocal microscopy was used to assess colocalization of α4 and CD82 in each cell line. Pearson's *r* was determined using ImageJ analysis ($r = 0.99$ for each image). (F) Control and CD82OE cells were treated with the α4β1-specific monovalent blocking peptide LDV, and adhesion to fibronectin was quantified using the fluorescence adhesion assay (*$p < 0.05$). Western blot analysis of total α4 protein expression in (G) control, CD82OE, and Palm-CD82OE cells or upon CD82 knockdown in KG1a cells transfected with (H) control siRNA, CD82 siRNA, and CD82 shRNA vectors. Western blot analysis of total β1 protein expression in (I) control, CD82OE, and Palm-CD82OE cells or upon CD82 knockdown in KG1a cells transfected with (J) control siRNA, CD82 siRNA, and CD82 shRNA vectors.

(Han *et al.*, 2012). As such, one mechanism by which CD82 could alter the surface expression of α4 is through changes in internalization. To monitor the internalization rate of the α4 integrin, we performed a fluorescence-quenching internalization assay using flow cytometry. After surface labeling of α4 at 4°C with a specific Alexa 488– conjugated antibody, we quenched the surface fluorescence of α4 with an anti–Alexa 488 antibody and quantified the remaining fluorescence as internalized α4 integrin. Figure 3, A and B, illustrates the percentage of total surface α4 internalized over time and demonstrates that CD82OE cells have reduced internalization compared with control cells. The internalization of α4 in Palm-CD82OE cells is similar to the internalization of CD82OE cells, suggesting that the palmitoylation of CD82 has no affect on the internalization of α4. Therefore one mechanism by which CD82 can modify the surface expression of integrins is by altering their endocytosis.

Once internalized, integrins can either be degraded through trafficking to the lysosome or recycled to the surface via the recycling endosome. To evaluate whether the reduced α4 internalization observed in the CD82OE cells (Figure 3A) could be due to changes in integrin recycling, we quantified α4 recovery to the surface. After the internalization and quench described for the endocytosis assay, we placed the cells back at 37°C for 30 min to evaluate the rate of α4 recycling. Figure 3C shows an increase in α4 recycling to the plasma membrane in both CD82OE and Palm-CD82OE cells. These data suggest that the decreased rate of α4 internalization observed with CD82 overexpression is likely mediated by an increase in α4 recycling. Together these data support a role for CD82 in regulating integrin expression through modulation of endocytosis and the recycling endosome pathway.

CD82 expression does not affect the α4β1 affinity state

Our data suggest a role for CD82 in the regulation of α4 integrin expression and its trafficking. However, in addition to differences in the expression of integrins, changes in cell adhesion can also be modulated by changes in integrin affinity. As such, we wanted to determine whether CD82 expression could change the α4β1 affinity state. To quantify potential differences in α4β1 affinity, we measured the binding affinity of LDV–fluorescein isothiocyanate (FITC) to cells

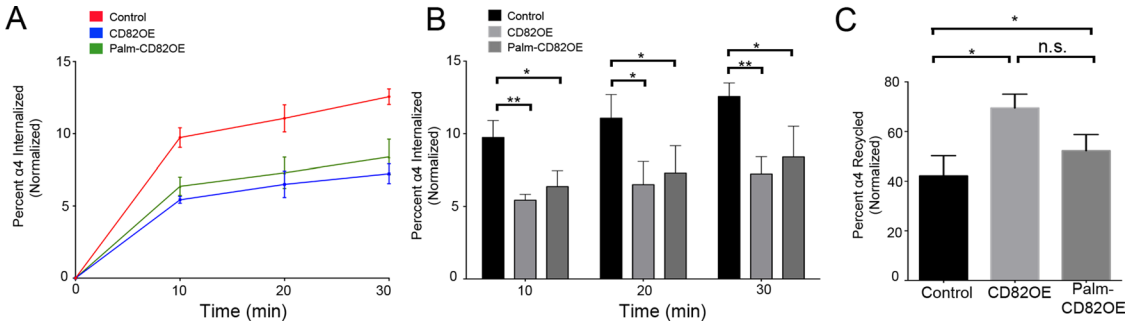

FIGURE 3: CD82 expression regulates α4 stability on the cell surface. (A, B) Control, CD82OE, and Palm-CD82OE cells were assessed for α4 internalization using a fluorescence-based internalization assay. Cells were labeled using an Alexa Fluor 488 integrin α4 antibody and allowed to internalize for 10, 20, and 30 min, and the surface fluorescence was quenched using an anti–Alexa Fluor 488 antibody. The remaining fluorescence indicates internalized protein, which was compared with 100% α4 surface labeling. (C) α4 recycling after 30 min was quantified from three independent experiments using a modified version of the internalization assay. Cells were allowed to internalize protein for 30 min and were then quenched and allowed to recycle protein back to the cell surface for 30 min. Surface fluorescence was quenched again, and the difference between the first and second quenches represents the amount of protein recycled back to the plasma membrane. Error bars, SD; $n = 3$ (*$p < 0.05$, **$p < 0.01$).

using a flow cytometer (Chigaev *et al.*, 2007). Binding isotherms or Langmuir plots were generated by incubating increasing concentrations of LDV-FITC with cells, and the measured fluorescence was fitted to a suitable nonlinear regression function to calculate the K_d values. These data suggest that CD82 overexpression does not statistically alter the affinity state of the α4β1 integrin (Supplemental Figure S5A). Next we used real-time flow cytometry to analyze the dissociation kinetics or "off rate" of LDV-FITC upon addition of a saturating, competitive concentration of unlabeled LDV (1 μM; Supplemental Figure S5B). The dissociation rate constant, K_{off}, was determined from the nonlinear fit and indicates that CD82 overexpression does not affect the off rate of LDV. The results taken together indicate that CD82 overexpression does not appear to alter the affinity state of the α4β1 integrin.

Palmitoylation of CD82 regulates its surface clustering

The overall strength of cellular adhesiveness is regulated by a combination of the affinity of individual integrins and their local density or surface geometry. Because tetraspanins are known to organize proteins into clusters or "webs," which could potentially alter the organization and density of surface integrins, we set out to evaluate the membrane distribution of CD82 and its effects on α4. Using the superresolution imaging technique dSTORM (Heilemann *et al.*, 2008), we reconstructed images of the single-molecule distribution of CD82 on the surface of each of the cell lines (Figure 4, A–C). From the magnified images, we were able to observe clusters of CD82 on the surface of control cells (Figure 4A), CD82OE cells (Figure 4B) and Palm-CD82OE cells (Figure 4C). To quantify the sizes of the identified CD82 clusters, we used the pair autocorrelation function (Figure 4, D–F). Previously described for dSTORM, the pair autocorrelation analysis establishes the probability of finding a molecule at a given distance from another molecule and does not depend on the number of times an average molecule is counted (Sengupta *et al.*, 2011; Veatch *et al.*, 2012). Applying this analytical method, we quantified the average radial protein cluster sizes of CD82 within the cell membrane. CD82 clusters measured on the control cells were significantly smaller (92 nm) than the average clusters in the CD82OE cells (140 nm; Figure 4G). Of interest, even though the CD82 surface expression is the same in CD82OE and Palm-CD82OE cells (Figure 1D), the measured cluster size of CD82 on the surface of Palm-CD82OE cells is significantly smaller (97 nm). These data illustrate that the palmitoylation sites within CD82 are critical for the molecular organization of CD82 into clusters. Although the role of palmitoylation in regulating tetraspanin clustering has been implicated from biochemical experiments (Berditchevski *et al.*, 2002; Charrin *et al.*, 2002; Yang *et al.*, 2002, 2004; Stipp, 2010), our data provide quantifiable imaging evidence that illustrates the importance of these sites for CD82 organization.

The α4 integrin is organized into small-scale clusters

Once we established the distribution of CD82 on each of our cell lines, we determined whether the expression and/or organization of CD82 had any effect on the clustering of the α4 integrin. Again, we used dSTORM imaging to assess potential changes in the α4 surface distribution between control, CD82OE, and the Palm-CD82OE cells. From the dSTORM images (Figure 5, A–C), we detect small-scale clusters of α4 in each cell line. Using the pair autocorrelation function just described, we fitted the α4 localization data (Figure 5, D–F) and extracted cluster sizes that were significantly smaller than those calculated for CD82 (Figure 5G). The average cluster size for each of the cell lines is ~35 nm. These data suggest that the α4 integrin is organized into small-scale membrane clusters on the order of 35 nm, which is not affected by CD82 expression.

Palmitoylation of CD82 regulates molecular density of α4 clusters

The contribution of integrin clusters to cellular adhesion is heavily dependent on their larger-scale molecular organization and protein density, which can alter the strength of the adhesive complex. Whereas the pair autocorrelation function is effective at quantifying the average uniform size of α4 clusters, the function output is representative of a singular α4 cluster. To assess the potential for CD82 to regulate the large-scale organization of α4, we analyzed the dSTORM images with the density-based spatial clustering of applications with noise (DBSCAN) data clustering algorithm (Ester *et al.*, 1996). DBSCAN quantifies cluster size in terms of cluster area, providing valuable information about the two-dimensionality of protein clusters (Kim *et al.*, 2013). This density-based clustering algorithm identifies clusters by evaluating the number of localizations that are within a density-reachable area and outputs the cluster sizes

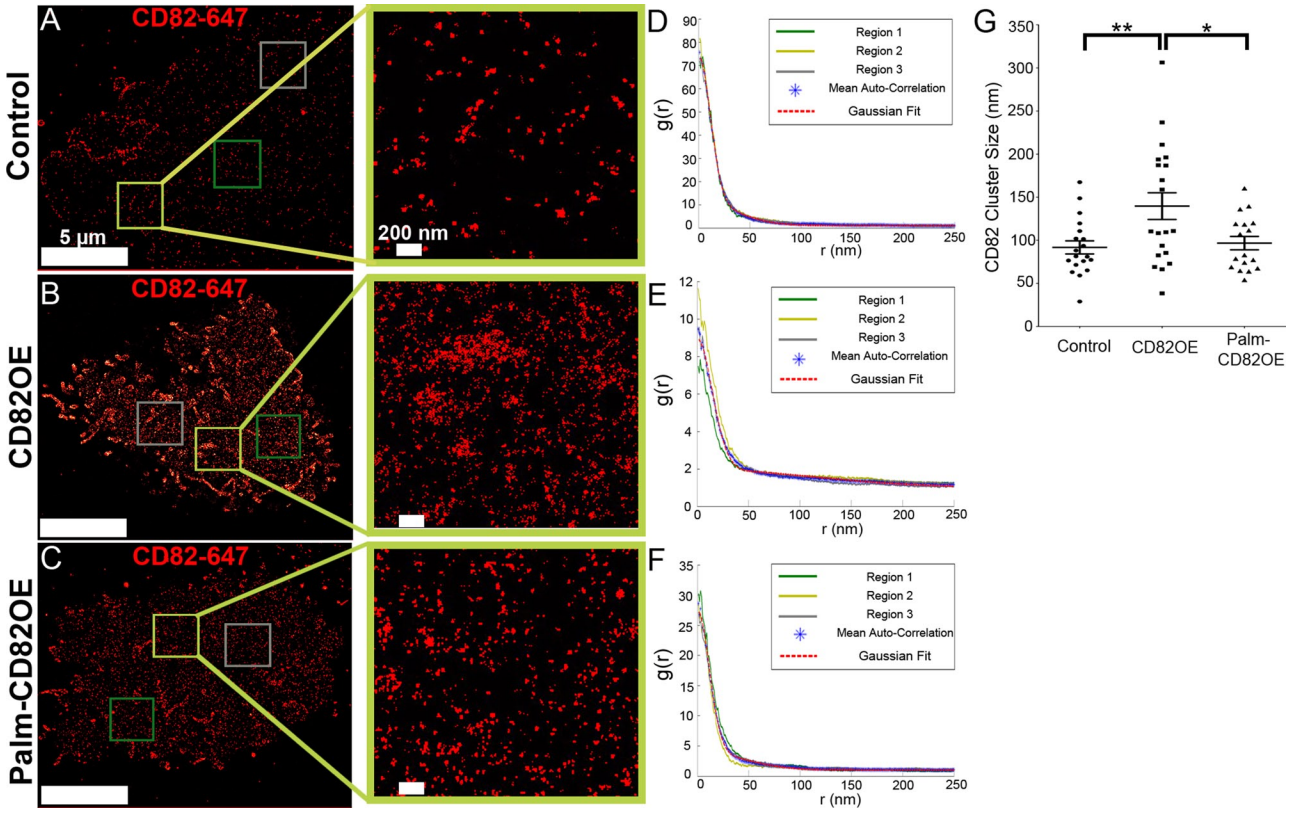

FIGURE 4: CD82 palmitoylation contributes to CD82 oligomerization. Reconstructed dSTORM images of representative (A) control, (B) CD82OE, and (C) Palm-CD82OE cells plated on fibronectin and labeled with an Alexa Fluor 647 anti–human CD82 antibody. CD82 cluster size was assessed using the pair autocorrelation function (Veatch *et al.*, 2012) for control (D), CD82OE (E), and Palm-CD82OE (F); this function determines the probability, $g(r)$, of localizing a molecule a given radius, r, away from another localized molecule. Radially averaged autocorrelation functions were calculated from three 3×3 µm regions of each cell as described in *Materials and Methods, Superresolution imaging*. The mean autocorrelation function from these three regions is shown in blue. (G) Average CD82 cluster size, σ_{Dom}, extracted from the fitting equation for each cell and plotted for each population of cells. Error bars, SEM; $n = 19$ cells for control, 20 cells for CD82OE, and 17 cells for Palm-CD82OE (**$p < 0.01$, *$p < 0.05$).

(in micrometers squared) found within a region of a cell. As such, the identified clusters are no longer dependent on a radial cluster size. Evaluating sections of the reconstructed dSTORM images from cells with approximately the same number of α4 localizations (Figure 6, A–C), we quantified the number of larger-scale α4 clusters, or "DB clusters." Using DBSCAN, we observed an increased number of total DB clusters of α4 in CD82OE and Palm-CD82OE cells (Figure 6G), which we attribute to the aforementioned increase in α4 surface expression in these cell lines (Figure 2A).

Integrins must organize into adhesive clusters that can resist the strong forces present at sites of adhesion while maintaining ligand engagement (Balaban *et al.*, 2001; Selhuber-Unkel *et al.*, 2008; Roca-Cusachs *et al.*, 2009). Therefore we used DBSCAN to quantify the organization of α4 localizations into clusters as a mechanism of increased HSPC adhesion. More specifically, we set out to determine the percentage of α4 localizations determined to be clustered, as well as the number of α4 localizations found within clusters. In both CD82OE and Palm-CD82OE cells, we calculated an increase in the percentage of localizations that are considered clustered (Figure 6H) by the DBSCAN. Furthermore, we found an increase in the average number of α4 localizations found within DB clusters for CD82OE as well as Palm-CD82OE cells (Figure 6I). These increases are likely due to our previous finding that CD82OE and Palm-CD82OE cells exhibit increased α4 surface expression compared with control cells (Figure 2A). Moreover, since both CD82OE and Palm-CD82OE cells show an increase in the percentage of α4 clustered as well as in number of α4 localizations within a cluster, these results are unlikely to account for the change in adhesion between CD82OE and Palm-CD82OE cells.

Adhesion complex stability can be strengthened by the tight packing of multiple integrins into clusters (Mammen *et al.*, 1998; Geiger *et al.*, 2001; Kiessling *et al.*, 2006; Selhuber-Unkel *et al.*, 2008). On further evaluation of the DBSCAN clusters, we observed a striking difference in the size of α4 clusters as well as in the spatial organization of α4 molecules within these clusters. When we magnify the reconstructed images to analyze the size and shape of the DB clusters (Figure 7, A–C), we find that CD82OE cells have smaller, more tightly packed clusters of α4 compared with control or Palm-CD82OE cells. (Additional, larger fields of view are illustrated in Supplemental Figure S6, A–C.) To assess differences in the distribution of clusters found using DBSCAN, we generated cumulative distribution plots of DB cluster sizes (Figure 7D and Supplemental Figure S7, A and B). The cumulative distribution plot illustrates the overall cluster sizes from all of the cells, which enables us to assess the percentage of clusters within a given size. Using the Kolmogorov–Smirnov test to assess whether two data sets differ significantly, we find that the distribution of clusters found in CD82OE cells differs from the distribution found in

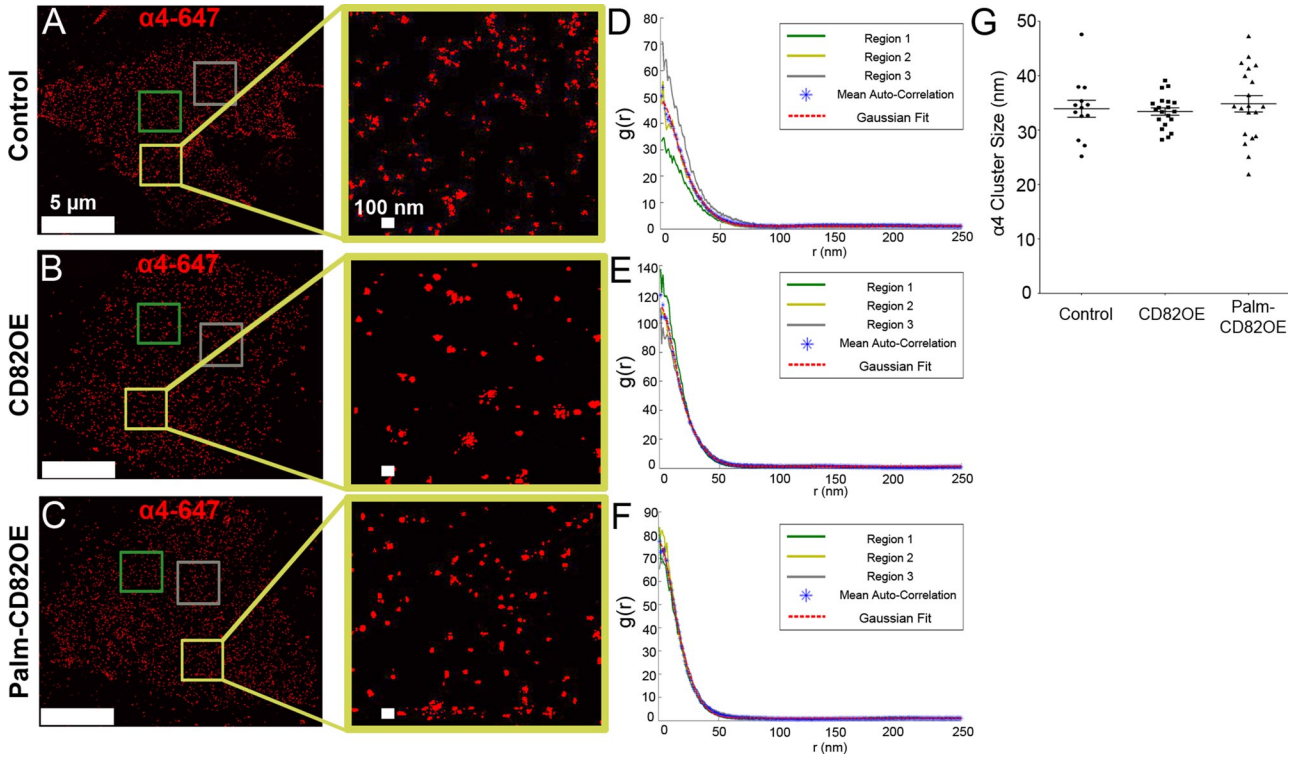

FIGURE 5: The α4 unit is organized into small-scale clusters. Reconstructed dSTORM images of representative (A) control, (B) CD82OE, and (C) Palm-CD82OE cells plated on fibronectin and labeled fluorescently for the α4 integrin subunit using a monoclonal α4 integrin primary antibody and goat anti-mouse Alexa Fluor 647 secondary antibody. The α4 cluster size was assessed using the pair autocorrelation function (Veatch *et al.*, 2012) for control (D), CD82OE (E), and Palm-CD82OE cells; this function determines the probability, $g(r)$, of localizing a molecule a given radius, r, away from another localized molecule. Radially averaged autocorrelation functions were calculated from three 3 × 3 μm regions of each cell as described in *Materials and Methods, Superresolution imaging* . The mean autocorrelation function from these three regions is shown in blue. (G) Average α4 cluster size, σ_{Dom}, extracted from the fitting equation for each cell and plotted for each population of cells. Error bars, SEM; $n = 13$ cells for control, 20 cells for CD82OE, and 20 cells for Palm-CD82OE.

control cells, as well as in Palm-CD82OE cells. These data suggest that α4 DB clusters present on CD82OE cells are smaller than those on control and Palm-CD82OE cells.

We next examined the size distribution of clusters found by DBSCAN by binning the data by α4 cluster area (micrometers squared). This allows us to extract the relative percentages of various-sized DB clusters detected and quantify differences in the types of DB cluster sizes identified, as well as their relative abundance. We found that in CD82OE cells, there is an increase in percentage of DB clusters that fall within the smaller, 0- to 0.0025-μm^2 bin (Figure 7F). In contrast, an increase in the larger DB clusters (>0.005 μm^2) is detected for Palm-CD82OE. In Figure 7E, we provide a visual reference for the length dimensions that would result in each of the square cluster areas. Taken together, these data indicate that there is a difference in the relative abundance of small and large α4 clusters between the overexpressing cell lines. Furthermore, these data suggest a functional difference between the ability of CD82OE and Palm-CD82OE cells to contribute to α4 cluster size. More specifically, the palmitoylation mutant form of CD82 is less effective at tightly packing the α4 molecules into a cluster, and so α4 clusters in Palm-CD82OE cells contain an increased proportion of clusters >0.005 μm^2.

In addition to identifying CD82-mediated changes in α4 cluster size, we also detected a difference in the spatial organization of α4 localizations within the clusters. To quantify these differences, we calculated the number of α4 localizations per unit cluster area of the cell (0.01 μm^2; Figure 7G). From these data, we found an increase in the average number of α4 localizations/0.01 μm^2 in CD82OE cells, indicating an increase in the number of α4 molecules packed into a smaller area of the membrane. When we compare these results to the α4 packing in Palm-CD82OE cells, we find that Palm-CD82OE does not promote compact lateral packing of α4 molecules within clusters. Next we assessed whether the presence of α4 ligand has an effect on CD82-mediated changes in α4 density. To quantify this potential difference, we completed the dSTORM imaging and analysis on cells that were plated on VCAM-1 (α4 ligand) or N-cadherin (nonligand). Of interest, our data indicate that the increase in α4 density measured in CD82OE cells occurs only when the cells are plated on an α4 ligand (Figure 7G and Supplemental Figure S8, A–C and G). When the cells are plated on N-cadherin, we no longer detect a change in integrin density (Figure 7G and Supplemental Figure S8, D–F and H). In combination, these data suggest a critical role of tetraspanins in promoting the organization of integrins into adhesion complexes, which allows for proper cell–ECM interactions. More specifically, our data suggest that CD82 mediates the tight packing of α4 into clusters upon ligand engagement, which increases the molecular density of α4 and enhances cell–matrix adhesion. Furthermore, our data indicate that CD82 palmitoylation is required for the effective formation of tightly packed integrin clusters.

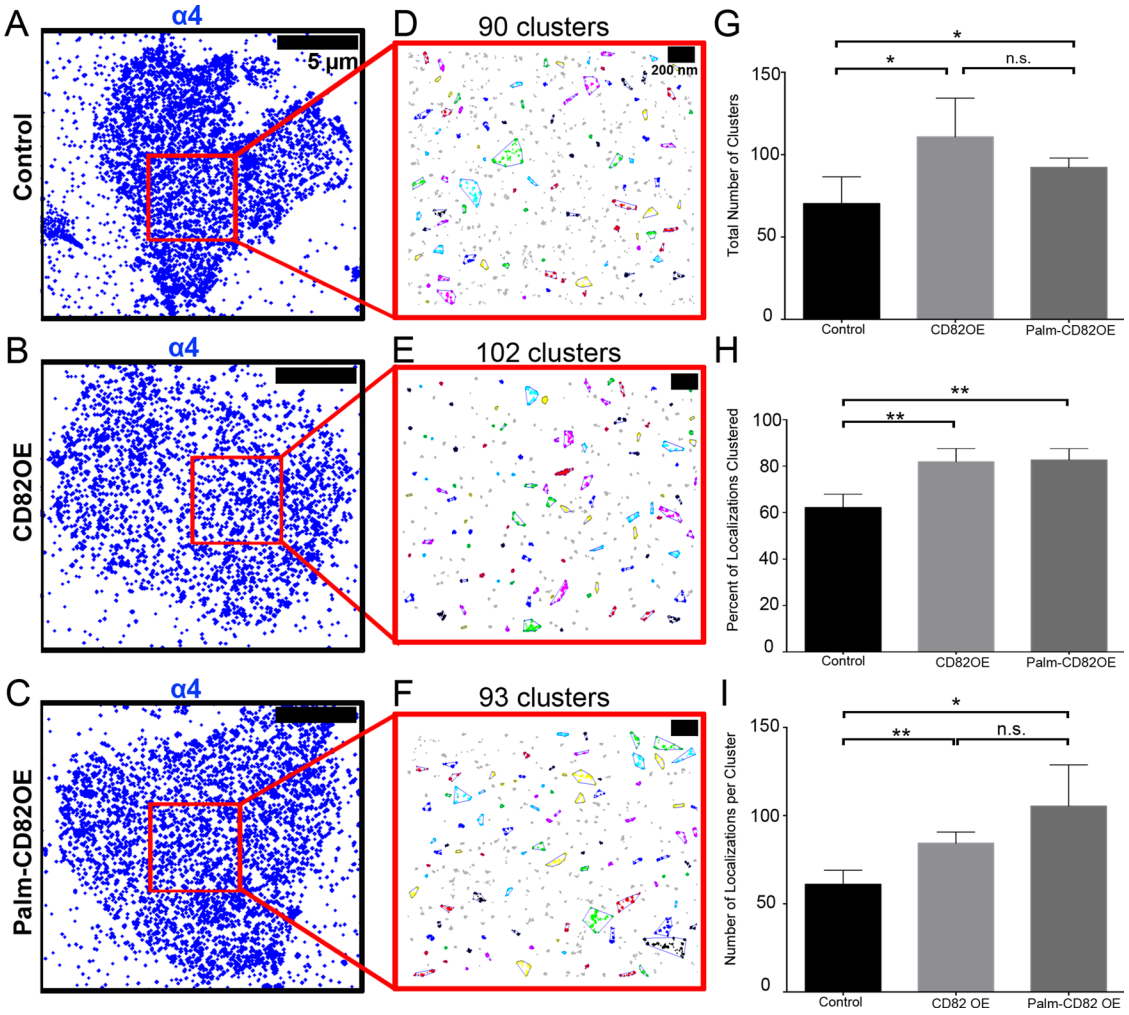

FIGURE 6: CD82 expression regulates α4 molecular organization. Reconstructed dSTORM images of representative (A) control, (B) CD82OE, and (C) Palm-CD82OE cells plated on fibronectin and labeled fluorescently for α4. (D–F) The DBSCAN algorithm was used to examine cluster organization within a subregion of the cells. The DBSCAN parameters used were $\varepsilon = 1$ pixel and $n = 30$ localizations. Colored localizations denote localizations organized into a cluster, and gray localizations indicate molecules not organized, as they did not meet the DBSCAN parameters. (G) Quantification of the total clusters determined by DBSCAN. (H) Quantification of the percentage of α4 localizations determined to be organized into clusters. (I) Average number of α4 localizations per cluster as determined by DBSCAN. Error bars, SD; $n = 4$ cells (*$p < 0.05$, **$p < 0.01$).

DISCUSSION

Tetraspanin–tetraspanin and tetraspanin–integrin interactions modify cell–cell and cell–matrix adhesion, although the molecular mechanisms that mediate these processes remain unclear. Our study provides strong evidence that the tetraspanin CD82 can regulate the membrane organization of integrins, resulting in the formation of tightly packed integrin "nanoclusters," which increases matrix adhesion. Moreover, if we inhibit lateral CD82 clustering by overexpressing a mutant form of CD82, which cannot be palmitoylated, we diminish the organization and molecular packing of α4 integrins and ultimately block cell–matrix adhesion. These results led us to propose a model in which CD82 TEMs serve to regulate the molecular density of integrins by recruiting them into and/or stabilizing them within plasma membrane clusters in a ligand-dependent manner (Figure 8).

Trafficking of HSPCs into and out of the bone marrow is essential throughout life to maintain homeostasis of the hematopoietic system and participate in innate immune responses. It is also critical in the clinical setting, where HSPCs can be isolated from normal donors and transplanted back into patients to replenish a compromised hematopoietic system. Previous work from our group identified the enrichment of CD82 at HSPC contact sites with osteoblasts, which led us to evaluate its potential role in HSPC/bone marrow interactions (Gillette *et al.*, 2009). In a follow-up study, we found that treatment of human $CD34^+$ cells with CD82 monoclonal antibodies inhibited $CD34^+$ cell adhesion and homing to the bone marrow, although the mechanism for this CD82-mediated effect on adhesion and homing remained unknown (Larochelle *et al.*, 2012). In this study, we evaluate how CD82 expression regulates cell adhesion, with particular focus on modifications in integrin interactions. First, we demonstrate a role for CD82 in cell adhesion, finding that CD82OE increases cell adhesion to fibronectin, whereas CD82KD results in decreased adhesion. Of interest, it is important to note that this CD82-mediated increase in fibronectin adhesion requires palmitoylation of CD82, since an increase in cell adhesion was not observed with the Palm-CD82OE mutant.

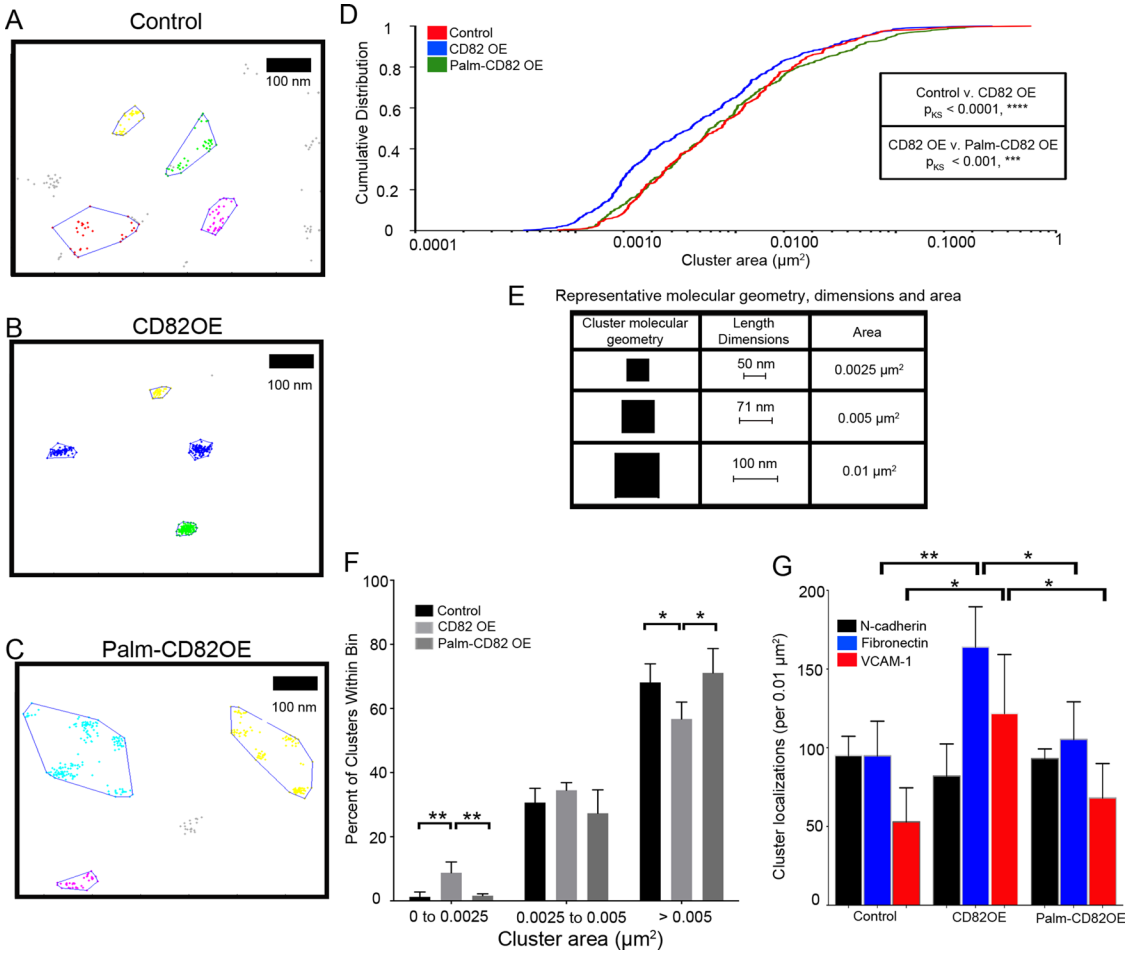

FIGURE 7: CD82 palmitoylation regulates the α4 density within clusters. Enlarged DBSCAN regions of (A) control, (B) CD82OE, and (C) Palm-CD82OE cells showing representative α4 clusters. (D) Cumulative distribution plot of the clusters compiled from $n = 4$ cells of each cell line plated on fibronectin; >250 clusters. Statistics determined using the Kolmogorov–Smirnov test. (E) Representative cluster geometry as depicted by black squares. Corresponding dimensions that give rise to cluster areas (0.0025, 0.005, and 0.01 μm^2) drawn to scale of images in A–C. (F) Percentage of total clusters that fall within the cluster area bins determined for cells plated on fibronectin. (G) Average number of α4 molecular localizations/0.01 μm^2 determined for cells plated on N-cadherin, fibronectin, and VCAM-1 using DBSCAN. Error bars, SD; $n = 4$ cells (*$p < 0.05$, **$p < 0.01$).

Previously the expression of CD82 was shown to modify adhesion through the αvβ3 (Ruseva *et al.*, 2009) as well as the α6 (He *et al.*, 2005) and β1 integrins (Jee *et al.*, 2007). We went on to evaluate CD82-mediated differences in integrin surface expression and identified changes in α4 expression. Signaling through the α4β1 integrin is known to regulate HSPC adhesion and homing to the bone marrow (Hartz *et al.*, 2011). For example, treatment of mice with α4-blocking antibodies results in HSPC mobilization into the blood (Papayannopoulou *et al.*, 1995; Craddock *et al.*, 1997). In addition, HSPC homing to the bone marrow is perturbed by α4-blocking antibodies, indicating that α4 plays a role in regulating HSPC/bone marrow niche interactions (Papayannopoulou *et al.*, 1995). Our results demonstrate that the CD82-mediated increase in fibronectin adhesion occurs primarily through the α4β1 integrin. Furthermore, we identified an increase in surface expression of α4 with CD82OE or Palm-CD82OE and a decrease in surface expression with CD82KD. Studies show that tetraspanins can modulate integrin surface distribution and function through the regulation of integrin internalization (Winterwood *et al.*, 2006; Liu *et al.*, 2007) and trafficking through the endosomal pathway (Caswell *et al.*, 2009). Previous studies show that the rate of α3β1 internalization is significantly reduced in CD151-silenced cells (Winterwood *et al.*, 2006). In addition, the YXXϕ motif in CD151 was identified as a structural element that determines the trafficking of its associated integrins (Liu *et al.*, 2007). In both CD82OE and Palm-CD82OE cells, we detect a decreased rate of α4 internalization, as well as an increased rate of α4 recycling, compared with control cells. These data suggest that CD82OE can increase the surface expression of integrins, independent of palmitoylation status, by enhancing their plasma membrane recycling rate. In combination, these data implicate a mechanism for our measured expression increase of surface α4. However, it is clear that α4 expression alone cannot account for the observed change in cell adhesion, since CD82OE and Palm-CD82OE cells express approximately the same amount of surface α4 yet have dramatically different adhesion abilities.

TEMS have been proposed to enhance cell adhesion by clustering functionally related molecules or tightly packing specific receptors into the plasma membrane (Yanez-Mo *et al.*, 2009). Palmitoylation can play a key role in the stable association of tetraspanins with each other (TEMs) and adhesion-related proteins. In fact, several

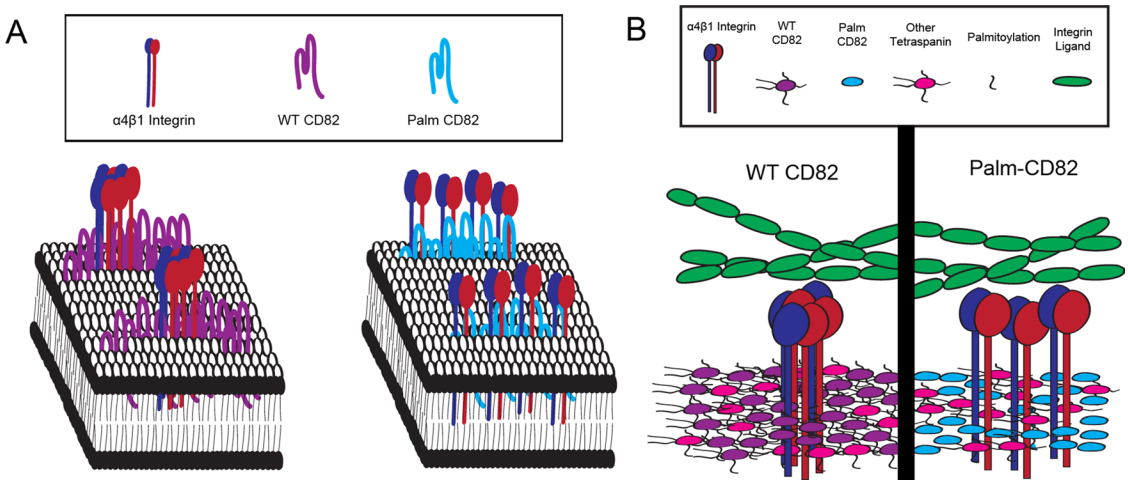

FIGURE 8: Proposed model for CD82 regulation of molecular clustering and protein density. On the basis of superresolution microscopy data, we propose a model in which CD82 expression and clustering modulate α4 protein density. (A) CD82OE facilitates the membrane clustering of CD82, which leads to larger CD82 clusters and more tightly packed α4 clusters. The detected increase in α4 density upon CD82OE depends on α4 ligand engagement. In contrast, Palm-CD82OE is unable to promote effective TEMs, which results in smaller CD82 clusters and reduced molecular density of α4. (B) The spatial arrangement of molecules within TEMs is essential for organizing adequate adhesion and signaling platforms, which are weakened by palmitoylation site mutation. The association of CD82 with other tetraspanins, a process strengthened by tetraspanin palmitoylation, could indirectly affect the molecular density of α4 clusters by disrupting the organization within the TEM required to establish effective packing of α4 molecules. The increased α4 molecular density results in α4 molecules within close proximity of one another, which contributes to the overall strength and activity of the adhesion complex.

reports show that mutation of the intracellular membrane-proximal cysteines reduces interactions between tetraspanins (Berditchevski *et al.*, 2002; Charrin *et al.*, 2002; Yang *et al.*, 2002, 2004; Zhou *et al.*, 2004; Delandre *et al.*, 2009; Stipp, 2010). In this study, we use the dSTORM superresolution imaging to visualize and quantitatively demonstrate palmitoylation-mediated alterations in tetraspanin organization. Our data indicate that mutation of the CD82 palmitoylation sites reduces the size of CD82 clusters within the plasma membrane and leads to changes in the membrane organization of the α4 integrin. Although previous work established that CD82 does not directly interact with α4β1 (Serru *et al.*, 1999), it is clear that α4β1 and CD82 exist within the same membrane complex (Mannion *et al.*, 1996). Therefore interaction of CD82 with other tetraspanins, which is stabilized by palmitoylation, likely contributes to the indirect linking of α4β1 into TEMs.

Previous work showed that tetraspanin association facilitates the recruitment of cell adhesion molecules such as VCAM and intercellular adhesion molecule into adhesive "nanoclusters" (Barreiro *et al.*, 2008). Similarly, CD81 was proposed to generate rapid adhesion strength to VCAM-1 through augmentation of α4β1 avidity (Feigelson *et al.*, 2003). More recently, CD37 was also shown to regulate the mobility and clustering of α4β1 in B cells (van Spriel *et al.*, 2012). Our clustering data indicate that CD82OE results in α4 clusters that are smaller in area than clusters found in control or Palm-CD82OE cells. However, despite the difference in average α4 cluster area, the number of α4 molecular localizations within each cluster remains the same. The molecular density of a protein cluster can be modified by altering the number of localizations found within a cluster area. Therefore fitting the same number of localizations into a smaller area results in the increased molecular density of α4 in CD82OE cells. The number and strength of bonds between integrins and ECM components can contribute to the overall strength of the adhesion complex (Maheshwari *et al.*, 2000). Our data suggest that it is the tight packing of α4 molecules, as promoted by CD82 upon α4 ligand engagement, that enhances the overall adhesive contribution of α4 clusters. The increase in laminin adhesion by CD82OE cells may also suggest that CD82 alters the clustering and potentially the density of laminin-binding integrins α3 and α6. Previous studies assessing the importance of integrin spacing for adhesive contribution postulated that proper positioning is necessary to maintain integrin linkages with one another, as well as adequate integrin binding to ECM components (Arnold *et al.*, 2004; Selhuber-Unkel *et al.*, 2008). Moreover, Arnold *et al.* (2004) showed that improper integrin-binding-site separation results in limited cell attachment due to restricted integrin clustering. In our study we find that CD82OE can facilitate the organization of α4 integrins into densely packed structures, implying the importance of α4 molecular density for cell adhesion. Furthermore, we speculate that the compromised α4 receptor clustering observed in Palm-CD82OE cells reduces adhesion by limiting the recruitment or stability of structural and/or signaling elements.

Among the tetraspanins, CD82 is largely studied in cancer, where its expression is inversely correlated with metastasis formation (Miranti, 2009; Zoller, 2009; Tsai and Weissman, 2011). The ability of CD82 to regulate metastasis is likely related to its ability to modulate integrin function, which we demonstrate in this study involves molecular density regulation. Taken together, the results indicate that CD82 can modify not only the assembly of membrane protein structures, but also the molecular concentration of integrins within these structures. Thus we propose that the molecular crowding of α4, which is regulated by CD82 and its palmitoylation state, modulates the overall adhesive strength of cells to the ECM. Finally, our detailed insight into how CD82 contributes to the coordinated molecular regulation and organization of α4 implicates CD82 as an attractive potential therapeutic target to improve HSPC mobilization and engraftment capabilities.

MATERIALS AND METHODS

Cell culture

KG1a human hematopoietic myeloid progenitor cells (CCL-246.1; ATCC, Manassas, VA) were cultured in RPMI 1640 medium (Mediatech, Manassas, VA), supplemented with 10% fetal bovine serum (FBS; Invitrogen, Carlsbad, CA), 2 mM L-glutamine (Invitrogen), 100 U/ml penicillin, and 100 μg/ml streptomycin (PenStrep; Invitrogen). Human microvascular endothelial cells were purchased and cultured as indicated by Cell Applications (San Diego, CA). Cells were incubated at 37°C, 5% humidity, and 5% CO_2.

Overexpression and knockdown vector constructs

To generate the mCherry-CD82 plasmid, CD82 was subcloned from the YFP-CD82 construct (Addgene, Cambridge, MA) into the mCherry-C1 Vector (Invitrogen) using the *Xho*I and *Sac*II restriction sites. The YFP-Palm-CD82 (CD82 palmitoylation mutant) construct was a generous gift from D. Derse (National Institutes of Health, Bethesda, MD; Mazurov *et al*., 2007). To increase the mCherry version of the construct, the PALM-CD82 insert was PCR amplified with the primers (forward) 5′-CTCGAGCGATGGGCTCAGCC-3′ and (reverse) 5′-CCGCGGAAGCTTTCAGTACTTGGG-3′ and inserted into the mCherry-C1 with the *Xho*I and *Sac*II restriction enzymes. The CD82 shRNA plasmid (Santa Cruz Biotechnology, Santa Cruz, CA) consisted of a pool of three to five plasmids encoding 19–25 nucleotides (plus hairpin). CD82-targeted siRNAs consisting of pools of three 20- to 25-nucleotide siRNA sequences and the scrambled control siRNA were also purchased from Santa Cruz Biotechnology.

Nucleofection

KG1a cells were transfected according to the manufacturer's instructions using the Lonza Nucleofection Kit (Lonza, Walkersville, MD). Stable cell lines expressing mCherry, mCherry-CD82, and mCherry-Palm–CD82 constructs were selected for with 500 μg/ml Geneticin (G418; Invitrogen). Stably expressing cells were isolated via fluorescence-activated cell sorting (University of New Mexico Facilities, Albuquerque, NM).

Flow cytometry

Cells were labeled in PAB buffer (phosphate-buffered saline [PBS] + 1% BSA + 0.02% sodium azide) for 30 min on ice with either Alexa Flour 647 CD82 (clone ASL-24; BioLegend, San Diego, CA), Alexa Flour 488 integrin α4 (clone 7.2R; R&D, Minneapolis, MN), FITC integrin α6 (clone GoH3; BioLegend), Alexa Flour 488 integrin α3 (clone ASC-1; BioLegend), APC integrin α5 (clone NKI-SAM-1; BioLegend), PE integrin α2 (clone HAS3; R&D), FITC integrin β7 (clone FIB27; BioLegend), or Alexa Flour 647 integrin β1 (clone TS2/16; BioLegend). Separate tubes of cells were labeled with Alexa Flour 488 mouse immunoglobulin G1 (IgG1), κ, isotype control (clone 11711; R&D), FITC rat IgG2a, κ, isotype control (clone RTK2758; BioLegend), Alexa Flour 647 mouse IgG1, κ, isotype control (clone MOPC-21; BioLegend), PE mouse IgG2a, κ, isotype control (clone MOPC-173; BioLegend), or APC mouse IgG2b, κ, isotype control (clone MPC-11; BioLegend). Cells were washed three times with PAB buffer and analyzed using Accuri C6 flow cytometer. Histograms were created using FlowJo software; fluorescence values were normalized to the mode.

Western blot and immunoprecipitation

Cells were lysed in RIPA buffer. Protein concentration was determined using the bicinchoninic acid (BCA) assay (Pierce, Rockford, IL). We subjected 25 μg of protein to 8 or 10% SDS–PAGE. The proteins were then transferred to a nitrocellulose membrane. Membranes were blocked with 5% dry milk in PBS with 0.22% Tween-20 for 1 h at room temperature. Membranes were then incubated with β-actin (clone AC-74; Sigma-Aldrich, St. Louis, MO), calnexin (clone C5C9, Cell Signaling, Beverly, MA), integrin α4 (clone EPR1355Y; Novus, Littleton, CO), integrin β1 (Cell Signaling), CD82 (clone ab66400; Abcam, Cambridge, MA), or integrin α6 (clone ab97760; Abcam) diluted in 5% milk/PBST overnight at 4°C. The membranes were washed three times for 10 min in PBS/0.22% Tween-20. Membranes were then incubated with peroxidase-conjugated AffiniPure goat anti-rabbit IgG or peroxidase-conjugated AffiniPure goat anti-mouse IgG secondary antibody diluted in 5% dry milk in PBS/0.22% Tween-20 for 1 h at room temperature. The membrane was washed three times for 10 min in PBS/0.22% Tween-20. Horseradish peroxidase conjugate enzymes were stimulated with SuperSignal West Pico Chemiluminescent Substrate (Pierce). Blots were imaged using the ChemiDoc XRS Imager (Bio-Rad, Hercules, CA) and analyzed using ImageJ (National Institutes of Health, Bethesda, MD) densitometry software. For immunoprecipitation experiments, BRIJ O10 cell lysates were incubated with CD82 antibody overnight at 4°C. Protein A/G Beads (Santa Cruz Biotechnology) were washed and added to the lysates for 30 min at room temperature. The supernatants were removed and the beads were washed three times before the beads and supernatants were analyzed for CD82 and α4 by Western blot as described.

Adhesion assay

We coated 96-well microplates with fibronectin (10 μg/ml in PBS; Millipore, Billerica, MA), collagen I (10 μg/ml in PBS; Sigma-Aldrich), laminin (10 μg/ml in PBS; BD Biosciences, Franklin Lakes, NJ), or 10% FBS as control. For the VCAM-1 adhesion assay, 10 μg/ml recombinant VCAM-1 (R&D) was used to coat wells. Cells were labeled for 20 min with 2 μM calcein AM fluorescent dye (Invitrogen) in Hank's buffered salt solution (HBSS). After two washes with HBSS, the cells were plated at 100,000 cells/well and incubated at 37°C for 2 h. The microplate was washed to remove nonadherent cells, and the remaining adherent cells were measured using a fluorescence plate reader with excitation wavelength of 488 nm and emission detected at 512 nm. Fluorescence data were then normalized to the mean fluorescence obtained for control cells. To measure α4β1-specific adhesion, cells were either treated with dimethyl sulfoxide or blocked with the monovalent peptide LDV (1 μM), which was a generous gift from Larry Sklar and Tione Buranda (University of New Mexico).

Immunofluorescence

Cells were fixed in 4% paraformaldehyde (PFA) and then blocked and permeabilized with PBS + 1.0% BSA + 0.1% Tween-20. Alexa Fluor 647-conjugated anti–human CD82 (clone ASL-24; BioLegend) and Alexa Fluor 488–conjugated anti–human integrin α4 (clone 7.2 R; R&D) were added to the sample. Immunofluorescence of VCAM-1 was completed with the mouse anti–human VCAM-1 primary antibody (AbD Serotec, Raleigh, NC) and the Alexa Fluor-488 goat anti-mouse secondary antibody (Life Technologies, Carlsbad, CA). Cells were labeled for 30 min. Cells were washed three times with PBS + 1% BSA and then imaged in an eight-well chamber slide. Cells were imaged by laser scanning confocal microscopy with a Zeiss Axiovert 100M inverted microscope (LSM 510) system (Carl Zeiss, Jena, Germany) using an excitation wavelength of 488 or 633 nm and a 63×/1.2 numerical aperture oil immersion objective. Image analysis was performed using the Zeiss LSM 510 software of ImageJ.

Internalization assay

Cells were labeled for 1 h on ice using an Alexa Fluor 488 integrin α4 antibody (clone 7.2R; R&D). Cells were washed three times using cold medium and resuspended in RPMI medium. An aliquot of cells was used to determine median fluorescence using the Accuri C6 flow cytometer; this is considered 100% surface labeling. The remaining cells were put into the incubator (37°C, 5% CO_2) for 10, 20, and 30 min. At the respective time point, 150,000 cells were moved to individual tubes. Cells were treated with 1 µg of anti–Alexa Fluor 488 antibody (clone A-11094; Invitrogen), which quenches surface fluorescence; cells were quenched on ice for 1 h, with >90% quenching efficiency. After quenching, cells were fixed for 20 min with 4% PFA. Median fluorescence in the FL-1 channel was read using Accuri C6 flow cytometer. Percentage internalized was calculated by dividing the median fluorescence intensity quenched value (normalized to background quench) by the median total α4 surface label intensity.

Recycling assay

Cells were labeled for 30 min on ice using an Alexa Fluor 488 integrin α4 antibody (clone 7.2R; R&D). Cells were washed three times using cold medium and resuspended in RPMI medium. Before allowing internalization, two aliquots of cells were removed. The first was to determine 100% α4 surface labeling. The second aliquot was quenched and fixed; this aliquot represents the quenched background fluorescence. The remaining cells were put back into the incubator (37°C, 5% CO_2) and allowed to internalize for 30 min. Cells were then treated with 1 µg of anti–Alexa Fluor 488 antibody (clone A-11094; Invitrogen) to quench surface fluorescence; cells were quenched on ice for 1 h. Cells were then moved back to the incubator (37°C, 5% CO_2) and allowed to recycle for 30 min. After 30 min, the samples were moved back on ice and quenched again for 1 h. Cells were then fixed with 4% PFA, and median fluorescence was determined using Accuri C6 flow cytometer. The difference between the internalized value and the recycled value gives the amount of α4 recycled back to the membrane. To calculate recycled α4, the fluorescence intensity values were normalized. Because fluorescence recycling changes are relatively small, quenched background was subtracted from internalized and recycled median fluorescence values. Percentage of α4 recycled was calculated by taking the difference between the normalized internalized and normalized recycled fluorescence median values and dividing this number by the normalized internalized value. This gives the percentage of α4 that was labeled, allowed to internalize for 30 min, and quenched upon recycling back to the plasma membrane.

Superresolution imaging

We used 25 µg/ml human plasma fibronectin (Millipore) diluted in PBS to coat the wells of an eight-well chamber slide for 20 min. We coated 15 µg/ml recombinant N-cadherin (R&D) diluted in PBS and wells for 30 min. We also used 10 µg/ml recombinant VCAM-1 (R&D) to coat wells for 1 h. Cells were then plated on the coated wells and incubated overnight at 37°C. The next day, cells were fixed with 4% PFA for 20 min, washed once with 1% BSA/PBS, and then blocked with 1% BSA/PBS for 1 h. For CD82 staining, cells were labeled with Alexa Fluor 647 anti–human CD82 antibody (1:125; clone ASL-24; BioLegend) diluted in 1% BSA/PBS. The wells were then washed three times with 1% BSA/PBS and fixed again with 4% PFA. For α4 staining, cells were first labeled with monoclonal α4 integrin primary antibody (1:200; clone Bu49; Thermo Scientific, Waltham, MA) diluted in 1% BSA/PBS for 1 h. The well was then washed three times with 1% BSA/PBS and subsequently labeled with goat anti-mouse Alexa Fluor 647 secondary antibody (1:200; Invitrogen) diluted in 1% BSA PBS for 1 h. The wells were then washed three times with 1% BSA/PBS and fixed again with 4% PFA.

Labeled cells were imaged in a reducing buffer including 50 mM β-mercaptoethylamine as a reducing agent. Reference beads were used as a reference point to stabilize the sample during imaging; drift corrections were performed using MCL NanoDrive stage controller. The sample was imaged for 10,000 frames using the microscope setup previously described (Huang *et al.*, 2011; van den Dries *et al.*, 2013). After molecule localization estimates and uncertainties were obtained, superresolution images were reconstructed using MATLAB analyses (Huang *et al.*, 2011).

The pair autocorrelation function (Veatch *et al.*, 2012) was used to analyze CD82 and α4 cluster size. Radially averaged autocorrelation functions were calculated from three 3×3 µm areas in each cell. Autocorrelation functions from the same cell were averaged and fitted to the functional form

$$g_{\text{meas}}(r) = B\left[\exp\left(-r^2/4\sigma_{\text{PSF}}^2\right)\right]/\left(4\pi\sigma_{\text{PSF}}^2\rho\right) + g(r>0)\,g_{\text{PSF}}$$

To decouple cluster sizes from broadening due to finite localization precision, domains are evaluated as two-dimensional Gaussian shapes, giving

$$g(r>0) = A\left[\exp\left(-r^2/4\sigma_{\text{Dom}}^2\right)\right]/4\pi\sigma_{\text{Dom}}^2$$

and therefore the fitting function

$$g_{\text{meas}}(r) = B\left[\exp\left(-r^2/4\sigma_{\text{PSF}}^2\right)\right]/4\pi\sigma_{\text{PSF}}^2\rho + AB\left\{\exp\left[-r^2/4\left(\sigma_{\text{Dom}}^2+\sigma_{\text{PSF}}^2\right)\right]\right\}/4\pi\left[\left(\sigma_{\text{Dom}}^2+\sigma_{\text{PSF}}^2\right)\rho\right]+1$$

Here A is the number of molecules per domain, B is the number of repeat observations per molecule, σ_{PSF} is the fluorophore localization precision, σ_{Dom} is the cluster size, and ρ is the observed localization density. The value for ρ was calculated directly from the selected regions, and A, B, σ_{PSF}, and σ_{Dom} were simultaneously estimated by performing a nonlinear least-squares fit of the average autocorrelation to $g_{\text{meas}}(r)$. The magnitude of $g(r)$ is a function of both the density and number of repeat observations of each molecule and can therefore differ with expression level, labeling efficiency, and imaging conditions, whereas the cluster size is extracted from the shape of the curve and is independent of these effects. The average cluster size for a population of cells was assessed statistically using Student's unpaired t test.

The DBSCAN cluster algorithm was used to assess larger-scale α4 clustering. A 56×56 pixel box (5.975×5.975 µm box) was examined for clustering. We used $\varepsilon = 1$ pixel (106.7 nm) and $n = 30$ localizations to examine α4 cluster area. To validate our parameters, we also tested the modified parameters $\varepsilon = 0.5$, $n = 30$ and $\varepsilon = 0.5$, $n = 20$ and saw the same trends of the cumulative distribution plots as assessed using the Kolmogorov–Smirnov test (Supplemental Figure S7, A and B).

Statistics

All experiments were performed at least three times independently. Results are expressed as mean ± SD or SEM. Student's t test was used for mean comparisons. The Kolmogorov–Smirnov test was used for comparison of cumulative distributions. Statistical analyses were performed using Prism 5 (GraphPad, La Jolla, CA). Significant differences are indicated using asterisks (*$p < 0.05$, **$p < 0.01$, ***$p < 0.001$, ****$p < 0.0001$).

ACKNOWLEDGMENTS

We acknowledge all of the funding sources that made this work possible. This includes Grant 13SDG14630080 from the American Heart Association (to J.M.G.), an American Cancer Society Institutional Research Grant, a Research Allocations Committee grant from the University of New Mexico, pilot funding from the University of New Mexico Cancer Center and the University of New Mexico Signature Program in Cardiovascular Disease and Metabolism, and a graduate student fellowship from the New Mexico Spatiotemporal Modeling Center (to C.M.T.).

REFERENCES

Arnold M, Cavalcanti-Adam EA, Glass R, Blummel J, Eck W, Kantlehner M, Kessler H, Spatz JP (2004). Activation of integrin function by nanopatterned adhesive interfaces. ChemPhysChem 5, 383–388.

Arroyo AG, Yang JT, Rayburn H, Hynes RO (1999). Alpha4 integrins regulate the proliferation/differentiation balance of multilineage hematopoietic progenitors in vivo. Immunity 11, 555–566.

Balaban NQ *et al*. (2001). Force and focal adhesion assembly: a close relationship studied using elastic micropatterned substrates. Nat Cell Biol 3, 466–472.

Barczyk M, Carracedo S, Gullberg D (2010). Integrins. Cell Tissue Res 339, 269–280.

Barreiro O, Zamai M, Yanez-Mo M, Tejera E, Lopez-Romero P, Monk PN, Gratton E, Caiolfa VR, Sanchez-Madrid F (2008). Endothelial adhesion receptors are recruited to adherent leukocytes by inclusion in preformed tetraspanin nanoplatforms. J Cell Biol 183, 527–542.

Bassani S, Cingolani LA (2012). Tetraspanins: interactions and interplay with integrins. Int J Biochem Cell Biol 44, 703–708.

Berditchevski F, Odintsova E, Sawada S, Gilbert E (2002). Expression of the palmitoylation-deficient CD151 weakens the association of alpha 3 beta 1 integrin with the tetraspanin-enriched microdomains and affects integrin-dependent signaling. J Biol Chem 277, 36991–37000.

Caswell PT, Vadrevu S, Norman JC (2009). Integrins: masters and slaves of endocytic transport. Nat Rev Mol Cell Biol 10, 843–853.

Charrin S, le Naour F, Silvie O, Milhiet PE, Boucheix C, Rubinstein E (2009). Lateral organization of membrane proteins: tetraspanins spin their web. Biochem J 420, 133–154.

Charrin S, Manie S, Oualid M, Billard M, Boucheix C, Rubinstein E (2002). Differential stability of tetraspanin/tetraspanin interactions: role of palmitoylation. FEBS Lett 516, 139–144.

Chigaev A, Waller A, Zwartz GJ, Buranda T, Sklar LA (2007). Regulation of cell adhesion by affinity and conformational unbending of alpha4beta1 integrin. J Immunol 178, 6828–6839.

Choi UJ, Jee BK, Lim Y, Lee KH (2009). KAI1/CD82 decreases Rac1 expression and cell proliferation through PI3K/Akt/mTOR pathway in H1299 lung carcinoma cells. Cell Biochem Funct 27, 40–47.

Coulombel L, Auffray I, Gaugler MH, Rosemblatt M (1997). Expression and function of integrins on hematopoietic progenitor cells. Acta Haematol 97, 13–21.

Craddock CF, Nakamoto B, Andrews RG, Priestley GV, Papayannopoulou T (1997). Antibodies to VLA4 integrin mobilize long-term repopulating cells and augment cytokine-induced mobilization in primates and mice. Blood 90, 4779–4788.

Delandre C, Penabaz TR, Passarelli AL, Chapes SK, Clem RJ (2009). Mutation of juxtamembrane cysteines in the tetraspanin CD81 affects palmitoylation and alters interaction with other proteins at the cell surface. Exp Cell Res 315, 1953–1963.

Ester M, Kreigel H-P, Sander J, Xu X (1996). A density-based algorithm for discovering clusters in large spatial databases with noise. In: Proceedings of the 2nd International Conference on Knowledge Discovery and Data Mining, Menlo Park, CA: AAAI Press, 226–231.

Feigelson SW, Grabovsky V, Shamri R, Levy S, Alon R (2003). The CD81 tetraspanin facilitates instantaneous leukocyte VLA-4 adhesion strengthening to vascular cell adhesion molecule 1 (VCAM-1) under shear flow. J Biol Chem 278, 51203–51212.

Geiger B, Bershadsky A, Pankov R, Yamada KM (2001). Transmembrane crosstalk between the extracellular matrix–cytoskeleton crosstalk. Nat Rev Mol Cell Biol 2, 793–805.

Gillette JM, Larochelle A, Dunbar CE, Lippincott-Schwartz J (2009). Intercellular transfer to signaling endosomes for targeted regulation within a bone marrow niche. Nat Cell Biol 11, 303–311.

Han SY *et al*. (2012). Tsp66E, the *Drosophila* KAI1 homologue, and Tsp74F function to regulate ovarian follicle cell and wing development by stabilizing integrin localization. FEBS Lett 586, 4031–4037.

Harburger DS, Calderwood DA (2009). Integrin signalling at a glance. J Cell Sci 122, 159–163.

Hartz B, Volkmann T, Irle S, Loechelt C, Neubauer A, Brendel C (2011). alpha4 integrin levels on mobilized peripheral blood stem cells predict rapidity of engraftment in patients receiving autologous stem cell transplantation. Blood 118, 2362–2365.

He B, Liu L, Cook GA, Grgurevich S, Jennings LK, Zhang XA (2005). Tetraspanin CD82 attenuates cellular morphogenesis through down-regulating integrin alpha6-mediated cell adhesion. J Biol Chem 280, 3346–3354.

Heilemann M, van de Linde S, Schuttpelz M, Kasper R, Seefeldt B, Mukherjee A, Tinnefeld P, Sauer M (2008). Subdiffraction-resolution fluorescence imaging with conventional fluorescent probes. Angew Chem Int Ed Engl 47, 6172–6176.

Hemler ME (2005). Tetraspanin functions and associated microdomains. Nat Rev Mol Cell Biol 6, 801–811.

Hemler ME (2008). Targeting of tetraspanin proteins—potential benefits and strategies. Nat Rev Drug Discov 7, 747–758.

Huang F, Schwartz SL, Byars JM, Lidke KA (2011). Simultaneous multiple-emitter fitting for single molecule super-resolution imaging. Biomed Opt Express 2, 1377–1393.

Jackson DY *et al*. (1997). Potent alpha 4 beta 1 peptide antagonists as potential anti-inflammatory agents. J Med Chem 40, 3359–3368.

Jee BK, Lee JY, Lim Y, Lee KH, Jo YH (2007). Effect of KAI1/CD82 on the beta1 integrin maturation in highly migratory carcinoma cells. Biochem Biophys Res Commun 359, 703–708.

Kiessling LL, Gestwicki JE, Strong LE (2006). Synthetic multivalent ligands as probes of signal transduction. Angew Chem Int Ed Engl 45, 2348–2368.

Kim I, Pan W, Jones SA, Zhang Y, Zhuang X, Wu D (2013). Clathrin and AP2 are required for PtdIns(4,5)P2-mediated formation of LRP6 signalosomes. J Cell Biol 200, 419–428.

Klein G (1995). The extracellular matrix of the hematopoietic microenvironment. Experientia 51, 914–926.

Kotha J, Longhurst C, Appling W, Jennings LK (2008). Tetraspanin CD9 regulates beta 1 integrin activation and enhances cell motility to fibronectin via a PI-3 kinase-dependent pathway. Exp Cell Res 314, 1811–1822.

Kovalenko OV, Yang X, Kolesnikova TV, Hemler ME (2004). Evidence for specific tetraspanin homodimers: inhibition of palmitoylation makes cysteine residues available for cross-linking. Biochem J 377, 407–417.

Larochelle A, Gillette JM, Desmond R, Ichwan B, Cantilena A, Cerf A, Barrett AJ, Wayne AS, Lippincott-Schwartz J, Dunbar CE (2012). Bone marrow homing and engraftment of human hematopoietic stem and progenitor cells is mediated by a polarized membrane domain. Blood 119, 1848–1855.

Li MQ, Hou XF, Shao J, Tang CL, Li DJ (2010). The DSC-expressed CD82 controls the invasiveness of trophoblast cells via integrinbeta1/MAPK/MAPK3/1 signaling pathway in human first-trimester pregnancy. Biol Reprod 82, 968–979.

Liu L, He B, Liu WM, Zhou D, Cox JV, Zhang XA (2007). Tetraspanin CD151 promotes cell migration by regulating integrin trafficking. J Biol Chem 282, 31631–31642.

Losordo DW *et al*. (2011). Intramyocardial, autologous CD34+ cell therapy for refractory angina. Circ Res 109, 428–436.

Maheshwari G, Brown G, Lauffenburger DA, Wells A, Griffith LG (2000). Cell adhesion and motility depend on nanoscale RGD clustering. J Cell Sci 113, 1677–1686.

Mammen M, Choi S-K, Wihitesides G (1998). Polyvalent interactions in biological systems: implications for design and use of multivalent ligands and inhibitors. Angew Chem Int Ed 37, 2754–2794.

Mannion BA, Berditchevski F, Kraeft SK, Chen LB, Hemler ME (1996). Transmembrane-4 superfamily proteins CD81 (TAPA-1), CD82, CD63, and CD53 specifically associated with integrin alpha 4 beta 1 (CD49d/CD29). J Immunol 157, 2039–2047.

Mazo IB, Massberg S, von Andrian UH (2011). Hematopoietic stem and progenitor cell trafficking. Trends Immunol 32, 493–503.

Mazurov D, Heidecker G, Derse D (2007). The inner loop of tetraspanins CD82 and CD81 mediates interactions with human T cell lymphotrophic virus type 1 Gag protein. J Biol Chem 282, 3896–3903.

Miranti CK (2009). Controlling cell surface dynamics and signaling: how CD82/KAI1 suppresses metastasis. Cell Signal 21, 196–211.

Nishiuchi R, Sanzen N, Nada S, Sumida Y, Wada Y, Okada M, Takagi J, Hasegawa H, Sekiguchi K (2005). Potentiation of the ligand-binding activity of integrin alpha3beta1 via association with tetraspanin CD151. Proc Natl Acad Sci USA 102, 1939–1944.

Oostendorp RA, Ghaffari S, Eaves CJ (2000). Kinetics of in vivo homing and recruitment into cycle of hematopoietic cells are organ-specific but CD44-independent. Bone Marrow Transplant 26, 599–566.
Papayannopoulou T, Craddock C, Nakamoto B, Priestley GV, Wolf NS (1995). The VLA4/VCAM-1 adhesion pathway defines contrasting mechanisms of lodgement of transplanted murine hemopoietic progenitors between bone marrow and spleen. Proc Natl Acad Sci USA 92, 9647–9651.
Papayannopoulou T, Nakamoto B (1993). Peripheralization of hemopoietic progenitors in primates treated with anti-VLA4 integrin. Proc Natl Acad Sci USA 90, 9374–9378.
Roca-Cusachs P, Gauthier NC, Del Rio A, Sheetz MP (2009). Clustering of alpha(5)beta(1) integrins determines adhesion strength whereas alpha(v) beta(3) and talin enable mechanotransduction. Proc Natl Acad Sci USA 106, 16245–16250.
Ruseva Z, Geiger PX, Hutzler P, Kotzsch M, Luber B, Schmitt M, Gross E, Reuning U (2009). Tumor suppressor KAI1 affects integrin alphavbeta3-mediated ovarian cancer cell adhesion, motility, and proliferation. Exp Cell Res 315, 1759–1771.
Scott LM, Priestley GV, Papayannopoulou T (2003). Deletion of alpha4 integrins from adult hematopoietic cells reveals roles in homeostasis, regeneration, and homing. Mol Cell Biol 23, 9349–9360.
Selhuber-Unkel C, Lopez-Garcia M, Kessler H, Spatz JP (2008). Cooperativity in adhesion cluster formation during initial cell adhesion. Biophys J 95, 5424–5431.
Sengupta P, Jovanovic-Talisman T, Skoko D, Renz M, Veatch SL, Lippincott-Schwartz J (2011). Probing protein heterogeneity in the plasma membrane using PALM and pair correlation analysis. Nat Methods 8, 969–975.
Serru V, Le Naour F, Billard M, Azorsa DO, Lanza F, Boucheix C, Rubinstein E (1999). Selective tetraspan-integrin complexes (CD81/alpha4beta1, CD151/alpha3beta1, CD151/alpha6beta1) under conditions disrupting tetraspan interactions. Biochem J 340, 103–111.
Sridhar SC, Miranti CK (2006). Tetraspanin KAI1/CD82 suppresses invasion by inhibiting integrin-dependent crosstalk with c-Met receptor and Src kinases. Oncogene 25, 2367–2378.
Stipp CS (2010). Laminin-binding integrins and their tetraspanin partners as potential antimetastatic targets. Expert Rev Mol Med 12, e3.
Taniguchi H, Toyoshima T, Fukao K, Nakauchi H (1996). Presence of hematopoietic stem cells in the adult liver. Nat Med 2, 198–203.
ter Huurne M, Figdor CG, Torensma R (2010). Hematopoietic stem cells are coordinated by the molecular cues of the endosteal niche. Stem Cells Dev 19, 1131–1141.
Tsai YC, Weissman AM (2011). Dissecting the diverse functions of the metastasis suppressor CD82/KAI1. FEBS Lett 585, 3166–3173.
van den Dries K, Schwartz SL, Byars J, Meddens MB, Bolomini-Vittori M, Lidke DS, Figdor CG, Lidke KA, Cambi A (2013). Dual-color superresolution microscopy reveals nanoscale organization of mechanosensory podosomes. Mol Biol Cell 24, 2112–2123.
van Spriel AB *et al.* (2012). The tetraspanin CD37 orchestrates the alpha(4) beta(1) integrin-Akt signaling axis and supports long-lived plasma cell survival. Sci Signal 5, ra82.
Veatch SL, Machta BB, Shelby SA, Chiang EN, Holowka DA, Baird BA (2012). Correlation functions quantify super-resolution images and estimate apparent clustering due to over-counting. PLoS One 7, e31457.
Wang XQ, Yan Q, Sun P, Liu JW, Go L, McDaniel SM (2007). Suppression of epidermal growth factor receptor signaling by protein kinase C activation requires CD82, caveolin-1, and ganglioside. Cancer Res 67, 9986–9995.
Winterwood NE, Varzavand A, Meland MN, Ashman LK, Stipp CS (2006). A critical role for tetraspanin CD151 in alpha3beta1 and alpha6beta4 integrin-dependent tumor cell functions on laminin-5. Mol Biol Cell 17, 2707–2721.
Xu C, Zhang YH, Thangavel M, Richardson MM, Liu L, Zhou B, Zheng Y, Ostrom RS, Zhang XA (2009). CD82 endocytosis and cholesterol-dependent reorganization of tetraspanin webs and lipid rafts. FASEB J 23, 3273–3288.
Yanez-Mo M, Barreiro O, Gordon-Alonso M, Sala-Valdes M, Sanchez-Madrid F (2009). Tetraspanin-enriched microdomains: a functional unit in cell plasma membranes. Trends Cell Biol 19, 434–446.
Yang X, Claas C, Kraeft SK, Chen LB, Wang Z, Kreidberg JA, Hemler ME (2002). Palmitoylation of tetraspanin proteins: modulation of CD151 lateral interactions, subcellular distribution, and integrin-dependent cell morphology. Mol Biol Cell 13, 767–781.
Yang X, Kovalenko OV, Tang W, Claas C, Stipp CS, Hemler ME (2004). Palmitoylation supports assembly and function of integrin-tetraspanin complexes. J Cell Biol 167, 1231–1240.
Zhang J, Li L (2008). Stem cell niche: microenvironment and beyond. J Biol Chem 283, 9499–9503.
Zhou B, Liu L, Reddivari M, Zhang XA (2004). The palmitoylation of metastasis suppressor KAI1/CD82 is important for its motility- and invasiveness-inhibitory activity. Cancer Res 64, 7455–7463.
Zoller M (2009). Tetraspanins: push and pull in suppressing and promoting metastasis. Nat Rev Cancer 9, 40–55.